J. Mater. Environ. Sci. 6 (1) (2015) 168-177
ISSN : 2028-2508
CODEN: JMESCN

Green synthesis of pyrazolo[3,4-b]pyridine derivatives by ultrasonic technique and their application as corrosion inhibitor for mild steel in acid medium

S.L. Gupta[1] , A. Dandia[1] ,Priyanka Singh[2], M.A. Quraishi[2]*

[1]*Centre of Advance Studies, Department of Chemistry,University of Rajasthan, Jaipur-302004 India*
[2] *Department of Chemistry, Indian Institute of Technology,Banaras Hindu University, Varanasi-221005*

Received 13 April 2014; Revised 17 October 2014; Accepted 19 October 2014.
**Corresponding Author. E-mail addresses: maquraishi.apc@itbhu.ac.in; Tel: (09307025126)*

Abstract
A green and convenient method using ultrasonic irradiation for the synthesis of pyrazolo[3,4-b]pyridine [PP] derivatives such as 4-(4-bromophenyl)-3-methyl-6-oxo-4,5,6,7-tetrahydro-2H-pyrazolo[3,4-b]pyridine-5-carbonitrile (PP-1), 4-(4-chlorophenyl)-3-methyl-6-oxo-4,5,6,7-tetrahydro-2H-pyrazolo[3,4-b]pyridine-5-carbonitrile (PP-2), 3-methyl-6-oxo-4-(3 phenoxyphenyl)-4,5,6,7-tetrahydro-2H-pyrazolo[3,4-b]pyridine-5-carbonitrile (PP-3) has been derived. The inhibition performance of the synthesized compounds on mild steel (MS) in 1M HCl has been investigated using weight loss, electrochemical impedance spectroscopy (EIS) and potentiodynamic polarization techniques. The results of electrochemical studies reveal that pyrazolo[3,4-b]pyridine derivatives are mixed type inhibitor and they inhibit corrosion by adsorption mechanism.

Key words: Corrosion inhibition, Mild steel (MS), Acid solution, Weight loss, Electrochemical measurements.

1. Introduction

Ultrasound technique is an eco-environmental technology in green chemistry. It is being used for last two decades for the synthesis of organic compounds. It has many advantages as compared with traditional methods. The procedure is more convenient and can be carried out in higher yields, shorter reaction time, under milder conditions and enables many chemical reactions to proceed which could not be carried out using traditional methods[1-2]. Pyrazolo[3,4-b]pyridines are heterocyclic compounds having biological activities such as antimicrobial [3], insecticidal [4], and anti-inflammator [5]. Thus, these compounds have potential for the treatment of several diseases, including bipolar disorder, diabetes, dementia, alzheimer's disease, schizophrenia, depression, and cancer [6]. Cartazolate, etazolate and tracazolate are anxiolytic drugs which are pyrazolopyridine derivatives and have unique pharmacological properties and used in scientific research [7].

Besides pharmacological properties Pyrazolo[3,4-b]pyridines also exhibit corrosion inhibition properties [8]. Mild steel suffers extensive corrosion in acidic media during pickling [9-13] .These compounds can adsorbed onto the MS surface and block the active surface sites to prevent corrosion [14-16]. In continuing our investigations on the application of ultrasound in organic synthesis, we wish to report here an efficient and convenient procedure for the synthesis of pyrazolo[3,4-b]pyridine derivatives using ultrasound technique to study their inhibition effect on corrosion of MS in 1M HCl using weight loss, electrochemical impedance spectroscopy (EIS) and potentiodynamic polarization techniques.

2. Experimental

2.1. Materials and Solutions

For weight loss and electrochemical studies the MS material having following composition (wt %): C 0.17%; Mn 0.46%; Si 0.026%; Cr 0.050%; P 0.012%; Cu 0.135%; Al 0.023%; Ni 0.05%; and balance Fe were used. For weight loss and electrochemical study following dimensions were 2.5 cm × 2 cm × 0.025 cm and 8 cm × 1 cm × 0.025 cm were used. The test solution of 1M HCl was prepared by diluting analytical grade 37% HCl with double distilled water. The stock solutions of inhibitors were prepared using 1% acetone in 1M HCl.

2.2. Weight loss measurements

Weight loss measurements were performed according to standard method [17]. The test coupons were immersed in 1M HCl (100 ml) in absence and presence of different concentration of inhibitors. After 3 h of immersion time the coupons were taken out, washed, dried and weighted accurately. The corrosion rate ($C_{R),}$ inhibition efficiency *(η%)* and surface coverage (θ) were determined by using following equations,

$$C_R\,(\mathrm{mm/y}) = \frac{87.6W}{atD} \quad (1)$$

$$\eta\% = \frac{C_R - {}^{i}C_R}{C_R}\ \mathrm{X}\ 100 \quad (2)$$

$$\theta = \frac{C_R - {}^{i}C_R}{C_R} \quad (3)$$

where W is the average weight loss of MS specimens, a is total surface area of MS specimen, t is the immersion time (3 h) and D is the density of MS in (gcm^{-3}), in equation (2) CR and ${}^{i}C_R$ is the corrosion rates of MS in the absence and presence of the inhibitors respectively.

2.3. Electrochemical measurements

The electrochemical experiments were performed by using three electrode cell, connected to Potentiostat/Galvanostat G300-45050 (Gamry Instruments Inc., USA). Echem Analyst 5.0 software package was used for data fitting. MS used as working electrode with an exposed area of 1 cm^2, platinum electrode as an auxiliary electrode, and saturated calomel electrode (SCE) as reference electrode. All potentials reported were measured versus SCE. Tafel curves were obtained by changing the electrode potential automatically from −0.25 V to +0.25 V versus open corrosion potential at a scan rate of 1.0 mVs^{-1}. Linear Polarization Resistance (LPR) experiments were done from −0.02 V to +0.02 V versus open corrosion potential at the scan rate of 0.125 mVs^{-1}. EIS measurements were performed under potentiostatic conditions in a frequency range from 100 kHz to 0.01 Hz, with amplitude of 10 mV AC signal. The experiments were carried out after an immersion period of 30 min in 1M HCl in absence and presence of different concentrations of PP derivatives.

2.4. General procedure for the synthesis of pyrazolo[3,4-b]pyridine [PP] derivatives

A mixture of appropriate benzaldehyde (10 mmol), ethyl cyanoacetate (10 mmol) and 3-amino-5-methylpyrazole (10 mmol) and 10 mol % *p*-TSA in 20 ml water was introduced in a heavy walled pear-shaped two-necked flask with non-standard taper outer joint. The flask was attached to a 12 mm tip diameter probe and the reaction mixture was sonicated for the specified period at 50% power of the processor and in a 4 s pulse mode till a solid product separates out. Completion of the reaction was monitored by TLC using n-hexane: ethyl acetate (7:3) as the eluent. All the reactions were invariably complete in 50-70 min. Upon completion, the reaction, the solid product was filtered washed with water, dried and recrystallised from ethanol [18]. The schematic representation is given in Scheme 1.

Scheme 1. Synthetic route for the preparation of PP derivatives

1.1. Physical methods of synthesized compounds

The melting points of PP derivatives were recorded on a Toshniwal apparatus and are uncorrected. The purity of compounds was checked on thin layers of silica gel in various non-aqueous solvent systems e.g. benzene:ethyl acetate(9:1), n-hexane: ethyl acetate (7:3). IR spectra (KBr) were recorded on a Shimadzu FT IR–8400s spectrophotometer and ^{1}HNMR and ^{13}CNMR spectra were recorded on a Bruker DRX-300 instrument at 300 and 75, respectively, in DMSO-d_6 relative to tetramethylsilane as an internal reference. Mass spectrum of representative compound was recorded on Waters Xevo Q-Tof spectrometer at 70 eV. Ultrasound irradiation was provided by ultrasonic processor probe (Processor SONOPROS PR-1000MP, OSCAR ULTRASONICS with power input 230V, 50 Hz, 4 Amps and power variac 0-230V and 3Amps) operating at 20 kHz, 750W with 6mm/12 mm tip diameter probes. All the supporting data is given in Table 1.

Table 1: Molecular structure and analytical data of PP derivatives

Structure	Analytical data
4-(4-bromophenyl)-3-methyl-6-oxo-4,5,6,7-tetrahydro-2H-pyrazolo[3,4-b]pyridine-5-carbonitrile (PP-1)	White powder; IR (KBr) cm^{-1}: 3572, 3294, 2244, 1706, 1540; ^{1}H NMR (300 MHz, DMSO-d_6) δ: 1.44 (s, 3H, CH_3), 4.53 (d, ^{3}J = 12.0 Hz, 1H, CH), 4.74 (d, ^{3}J = 11.7 Hz, 1H, CH), 7.34-7.67 (m, 4H, ArH), 10.99 (s, 1H, NH_{amid}), 12.30 (brs, 1H, $NH_{pyrazole}$) ppm. ^{13}C NMR (75 MHz, DMSO-d_6) δ: 10.04, 36.26, 43.74, 100.48, 117.51, 122.02, 130.64, 132.23, 135.78, 139.08, 147.71, 163.26 ppm; +ESI MS (m/z): 331 $[M+H]^+$.
4-(4-chlorophenyl)-3-methyl-6-oxo-4,5,6,7-tetrahydro-2H-pyrazolo[3,4-b]pyridine-5-carbonitrile (PP-2)	White powder; IR (KBr) cm^{-1}: 3572, 3294, 2244, 1706, 1540; ^{1}H NMR (300 MHz, DMSO-d_6) δ: 1.47 (s, 3H, CH_3), 4.49 (d, ^{3}J = 12.0 Hz, 1H, CH), 4.68 (d, ^{3}J = 11.7 Hz, 1H, CH), 7.13-7.61 (m, 4H, ArH), 10.95 (s, 1H, NH_{amid}), 11.99 (brs, 1H, $NH_{pyrazole}$) ppm. ^{13}C NMR (75 MHz, DMSO-d_6) δ: 10.01, 36.67, 43.78, 100.51, 117.50, 129.27, 130.75, 132.90, 135.74, 138.56, 147.67, 163.33 ppm; +ESI MS (m/z): 287 $[M+H]^+$.
3-methyl-6-oxo-4-(3-phenoxyphenyl)-4,5,6,7-tetrahydro-2H-pyrazolo[3,4-b]pyridine-5-carbonitrile (PP-3)	White powder; IR (KBr) cm^{-1}: 3568, 3284, 2238, 1705, 1542; ^{1}H NMR (300 MHz, DMSO-d_6) δ: 1.48 (s, 3H, CH_3), 4.50 (d, ^{3}J = 12.0 Hz, 1H, CH), 4.69 (d, ^{3}J = 12.0 Hz, 1H, CH), 7.14-7.63 (m, ArH, 9H), 10.96 (s, 1H, NH_{amid}), 12.00 (brs, 1H, $NH_{pyrazole}$) ppm. ^{13}C NMR (75 MHz, DMSO-d_6) δ: 9.92, 36.61, 43.98, 100.83, 115.91, 116.19, 116.77, 117.54, 129.77, 130.87, 135.69, 135.78, 136.61, 147.62, 160.48, 163.55 ppm; +ESI MS (m/z): 345 $[M+H]^+$.

2. Results and discussion

2.1. Weight loss measurements

2.1.1. Effect of inhibitor concentration

The effects of PP derivatives at different concentration were studied by weight loss technique. This method was used to found the optimum concentration of investigated inhibitors [19-20]. The observations by weight loss studies were given in Table 2 show that corrosion rate of MS decreases and inhibition efficiency increases on addition of different concentration of inhibitor. The maximum inhibition efficiency of 89.04% was obtained for PP-1.

2.1.2. Effect of Temperature

The thermodynamic activation parameters such as activation energy (E_a), enthalpy (ΔH^*), and entropy (ΔS^*) were studied at temperature308–338 K. The inhibition efficiency of PP derivatives decreases with increase in temperature. The decrease in inhibition efficiency with rise in temperature may be attributed due to desorption

of inhibitor molecule from the MS surface. The parameters such as activation energy (E_a), enthalpy (ΔH^*), and entropy (ΔS^*) were evaluated to explain the thermodynamics of corrosion reaction and dependence of corrosion rate with variation in temperature given in Table 3.

Table 2: Parameters obtained from weight loss measurements for MS in 1M HCl containing different concentrations of PP derivatives

Inhibitors	Concentrations (ppm)	Corrosion rate (mm/y)	Surface coverage θ	η%
Blank	0.0	77.9	-	-
PP-1	25	15.9	0.79	79.52
	50	13.9	0.82	82.14
	75	10.7	0.86	86.19
	100	9.4	0.87	89.04
PP-2	25	17.4	0.77	77.61
	50	14.4	0.81	81.42
	75	11.5	0.85	85.23
	100	10.3	0.86	87.14
PP-3	25	21.5	0.72	72.38
	50	17.0	0.78	78.09
	75	14.8	0.80	80.95
	100	12.2	0.84	84.28

The activation energy can be calculated using following equation,

$$\ln(C_R) = \frac{-E_a}{RT} + A \quad (4)$$

where E_a is the activation energy for corrosion of MS in 1M HCl, R is the gas constant, A the Arrhenius pre-exponential factor and T is the absolute temperature.

Table 3: Activation parameters in absence and presence of optimum concentration of PP derivatives

Inhibitors	Ea (kJmol^{-1})	ΔHa ((kJmol^{-1})	ΔSa (JK^{-1}mol^{-1})
Blank	29.10	26.42	-123.27
PP-1	55.40	52.70	-56.14
PP-2	54.99	52.14	-56.80
PP-3	53.64	50.83	-58.81

A plot of the corrosion rate ln C_R vs 1000/T gives a straight line as shown in Figure 2. The values of E_a in 1M HCl in absence and presence of PP derivatives are determined from the slope by plotting the values obtained. The enthalpy and entropy of activation (ΔH^* and ΔS^*) can be calculated by given equation,

$$C_R = \frac{RT}{Nh}\exp\left(\frac{\Delta S^*}{R}\right)\exp\left(-\frac{\Delta H^*}{RT}\right) \quad (5)$$

where h is Plank constant and N is Avogadro's number.

A plot of ln (C_R /T) against 1000/T shown in Figure 3 gave straight lines with a slope of ($-\Delta H^*/R$) and an intercept of [(ln(R/Nh)) + ($\Delta S^*/R$)] from which the values of ΔH^* and ΔS^* are calculated.

Higher values of E_a and ΔH^* in the presence of inhibitor indicate more energy is required for the dissolution of MS in 1M HCl in presence of inhibitors. The positive signs of ΔH^* reflect the endothermic nature of dissolution process. The higher values of ΔS^* for inhibited solutions than for uninhibited solution might be the result of the adsorption of PP molecules from 1M HCl solution, which could be regarded as a quasi substitution process between the inhibitor molecules in the aqueous phase and water molecules on the MS surface[21-22]

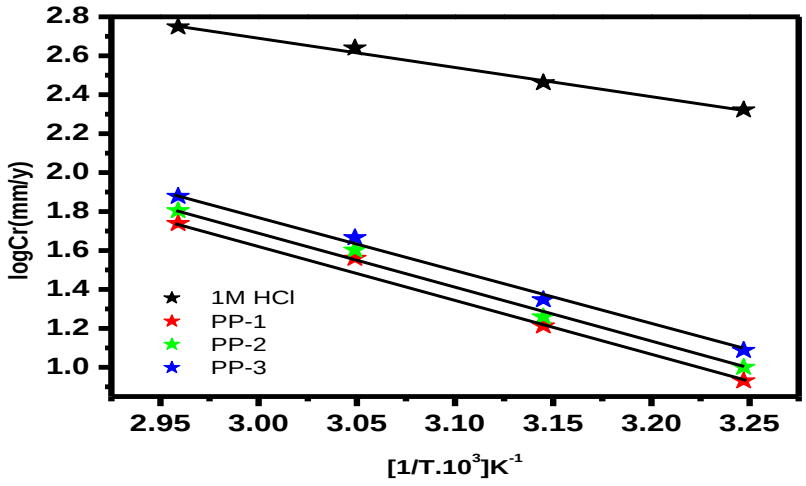

Figure 2: Arrhenius plots of log C_R vs. 1000/T for MS in 1M HCl in the absence and the presence of PP derivatives at optimum concentration

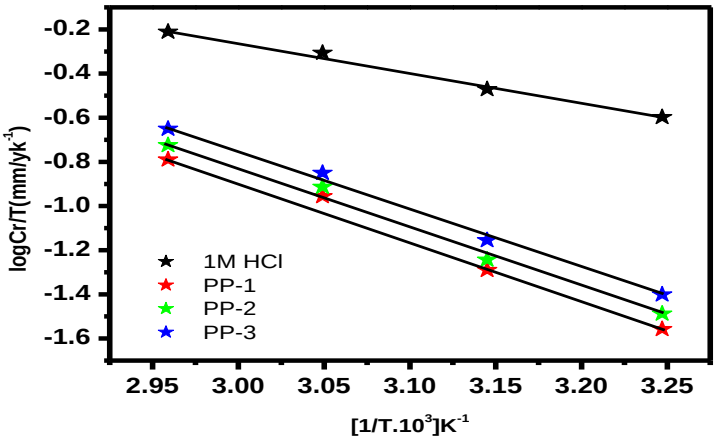

Figure 3: Arrhenius plots of log C_R/T vs. 1000/T for MS in 1M HCl in the absence and presence of PP derivatives at optimum concentration.

2.1.3. *Adsorption isotherm*

Adsorption isotherm gives the basic information about the interaction of inhibitor molecules with MS surface. Inhibitors are adsorbed on MS surface containing a fixed number of adsorption sites rapidly and form a protective layer on MS surface. The surface coverage (θ) was calculated according to equation (3). A correlation between (θ) and inhibitor concentration (C_{inh}) can be represented by the Langmuir adsorption isotherm,

$$K_{ads} = \frac{\theta}{C(1-\theta)} \quad (6)$$

The equation can be rearrange as,

$$\frac{C_{(inh)}}{\theta} = \frac{1}{K_{(ads)}} + C_{(inh)} \quad (7)$$

The value of surface covered (θ) was tested graphically for fitting suitable isotherms including Frumkin, Temkin and Langmuir. Best fit was obtained for Langmuir isotherm shown in Figure 4 with regression coefficient R^2 value (0.99935 to 0.99989) which is nearly one.

K_{ads} is related to the standard free energy of adsorption ΔG_{ads} by the following equation,

$$\Delta G_{ads} = -RT \ln(55.5 K_{ads}) \quad (8)$$

where *R* is the gas constant and *T* is the absolute temperature. The value of 55.5 is the concentration of water in solution in mol L^{-1}.

The calculated values for ΔG_{ads} at optimum concentration ranges from -36.4 to-35.3 KJ mol^{-1} at 308 K which indicates that the adsorption of the inhibitor on MS surface may involve both physical as well as chemical adsorption [23].

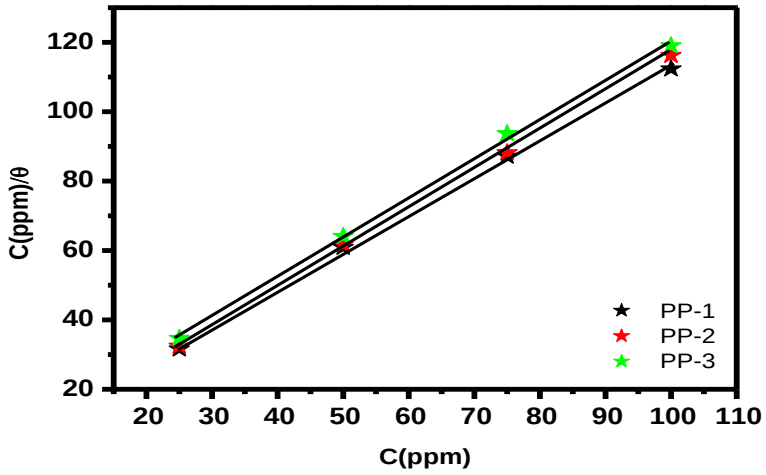

Figure 4: Langmuir isotherms for adsorption of PP derivatives on MS surface in 1M HCl

2.2. Electrochemical measurements

2.2.1. Potentiodynamic polarization measurements

The polarisation curves for MS in 1 M HCl in absence and presence of inhibitors are shown in Figure 5 and electrochemical parameters such as corrosion potential (E_{corr}), corrosion current density (I_{corr}), anodic (β_a) and cathodic (β_c) slopes are listed in Table 4. The inhibition efficiency (η %) values were calculated from the relation:

$$\eta\% = \frac{I_{corr} - I_{corr(i)}}{I_{corr}} \times 100 \quad (9)$$

where I_{corr} and $I_{corr(i)}$ are the corrosion current density in absence and presence of inhibitors.

Table 4: Polarization Parameters of MS in 1M HCl Solution at different concentration of PP derivatives

Inhibitors	Concentrations (ppm)	I_{corr} (μAcm^{-2})	E_{corr} (mV/SCE)	β_a (mV/dec)	β_c (mV/dec)	η%
Blank	0.0	1390	-445	82	118	-
PP-1	25	291	-483	58	156	79.06
	50	221	-493	77	157	84.10
	75	156	-495	78	154	88.77
	100	126	-501	82	148	90.93
PP-2	25	327	-493	72	141	76.47
	50	226	-496	46	80	83.74
	75	169	-506	131	306	87.84
	100	130	-513	97	175	90.64
PP-3	25	444	-490	64	149	68.05
	50	394	-495	68	143	71.65
	75	299	-499	78	160	78.41
	100	160	-485	60	169	88.48

It is seen from results that addition of inhibitors causes decrease in I_{corr} values. The maximum reduction of I_{corr} was obtained for AP-1 which gave an inhibition efficiency of 90.93% at 100 ppm [24]. The addition of PP derivatives do not alter the value of E_{corr} significantly which was not more than 85 mV as compared to blank 1M HCl indicating the mixed type of inhibiting behaviour of inhibitors[25-26] . The change in β_a and β_c values indicates that adsorption of inhibitor modify the mechanism of anodic dissolution as well as cathodic hydrogen evolution.

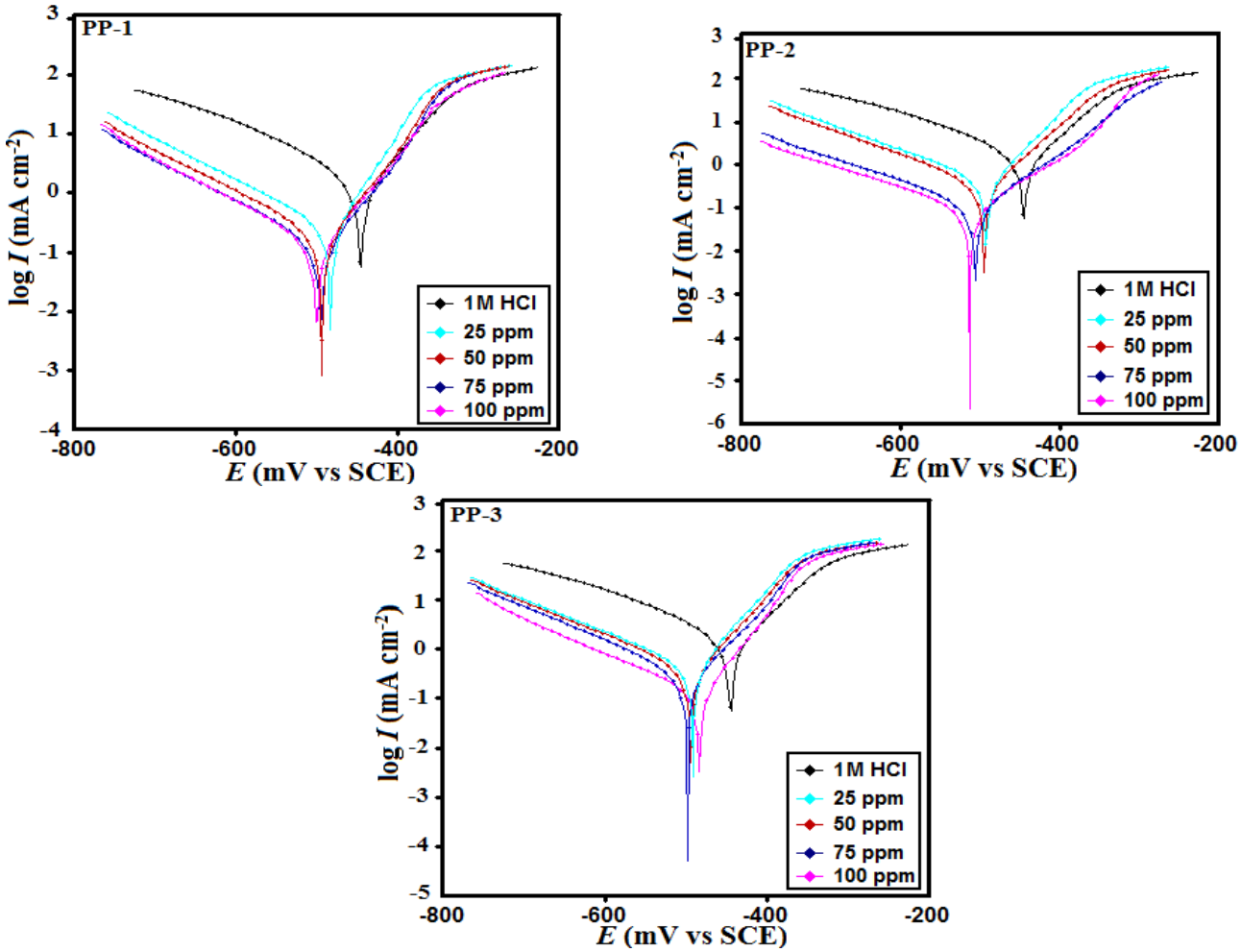

Figure 5: Tafel curves for MS in 1M HCl without and with different concentrations of PP derivatives

2.2.2. *Electrochemical impedance spectroscopy (EIS)*

The impedance behaviour of MS in 1M HCl with and without addition of PP derivatives is given in Figure 6. The equivalent circuit model used for analysis is shown in Figure 7. It consist of solution resistance (*R*s), the charge-transfer resistance of the interfacial corrosion reaction (*R*ct) and the constant phase angle element (CPE). The inhibition efficiency was calculated using charge transfer resistance (R_{ct}) as follows,

$$\eta\% = \frac{R_{ct(inh)} - R_{ct}}{R_{ct(inh)}} \times 100 \qquad (10)$$

where $R_{ct(inh)}$ and R_{ct} are the values of charge transfer resistance in presence and absence of inhibitors in 1M HCl respectively.

The addition different concentration of inhibitor increases R_{ct} and decreases C_{dl} with respect to blank. The increase in R_{ct} values is attributed due to increase in resistance and which causes decrease in C_{dl} shown in Table 5 [27-28]. The values of double layer capacitance, C_{dl} were calculated from equation.

$$C_{dl} = Y_0 (\omega_{max})^{n-1} \qquad (11)$$

where Y_0 is CPE coefficient, n is CPE exponent (phase shift), ω is the angular frequency. The thickness of this protective layer (d) is correlated with C_{dl} by the following equation,

$$C_{dl} = \frac{\varepsilon \varepsilon_o A}{d} \quad (12)$$

where ε is the dielectric constant and ε_0 is the permittivity of free space and A is surface area of the electrode. Equation (7) suggests that C_{dl} is inversely proportional to the thickness of protective layer d [29].

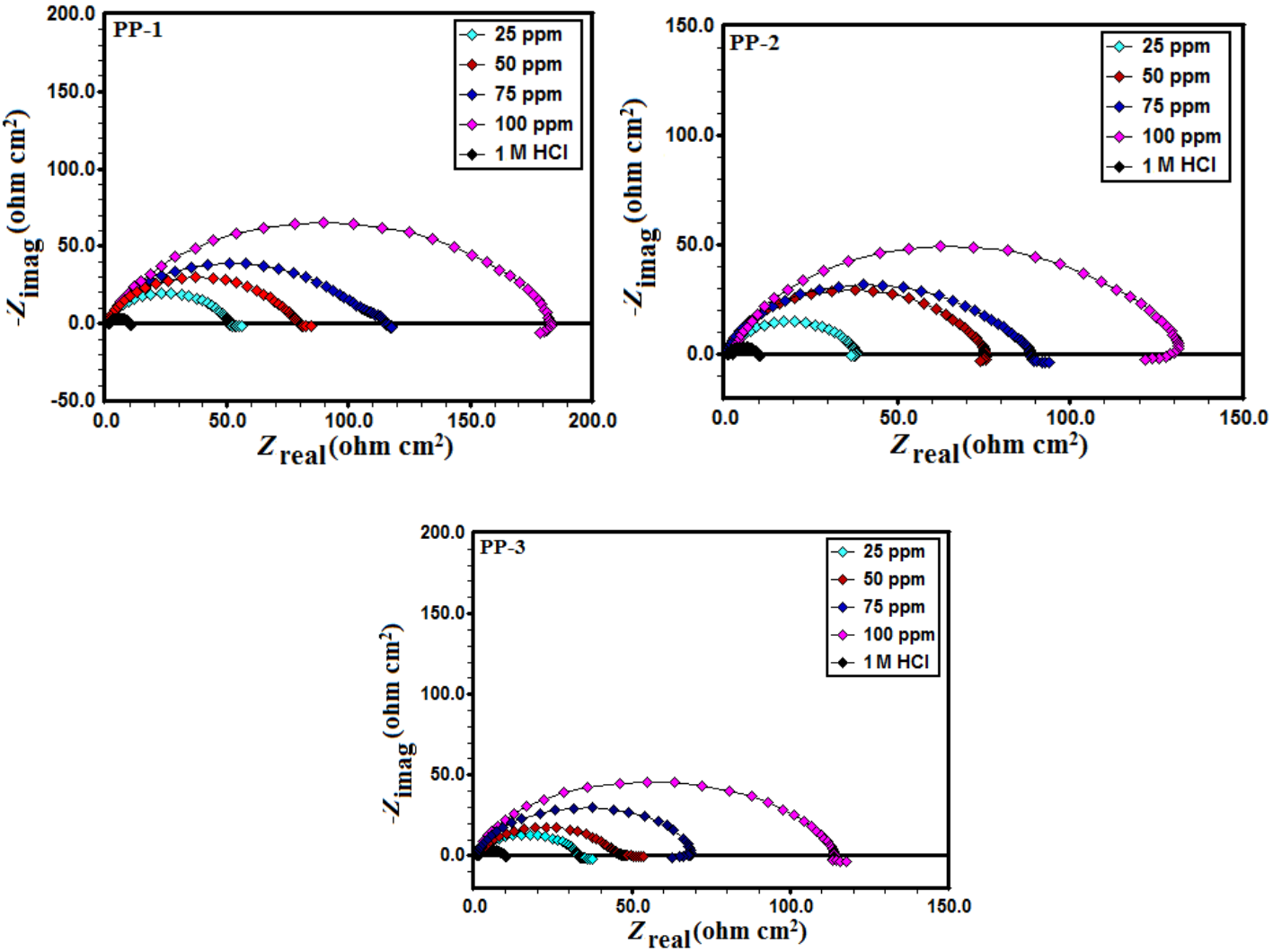

Figure 6: Nyquist plots for MS in 1M HCl without and with different concentrations of PP derivatives

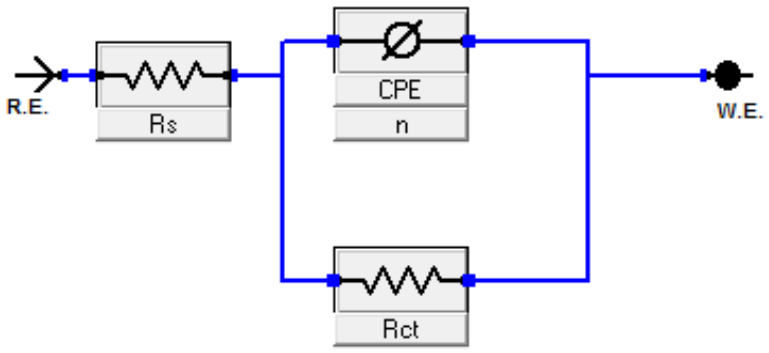

Figure 7: Equivalent circuit model used to fit the EIS data

Bode plot [log |*Z*| Vs log *f*] and phase angle plot [α° Vs log *f*] are shown in Figure 8. It is seen an ideal capacitor behavior would result if a slope value attains –1 and phase angel values attain -90° [30]. The deviation in slope and phase angle values in presence of PP inhibitors shows anti corrosion performance.

Table 5: Electrochemical impedance parameters for mild steel in 1M HCl in the absence and presence of different concentrations of PP derivatives

Inhibitors	Concentrations	$R_s(\Omega)$	$R_{ct}(\Omega\ cm^2)$	n	Y_o (μFcm^{-2})	C_{dl}	$\eta\%$
Blank	0.0	1.02	9.0	0.822	50	106	-
PP-1	25	.849	50.1	0.871	130	67	82.04
	50	.963	79.4	0.851	108	48	88.67
	75	.957	107.6	0.844	130	52	91.63
	100	1.267	177.3	0.831	146	50	94.92
PP-2	25	.786	36.4	0.865	133	69	75.33
	50	.852	72.7	0.874	112	56	87.63
	75	.829	85.3	0.858	117	53	89.45
	100	1.305	125.8	0.862	119	52	92.85
PP-3	25	.755	31.8	0.890	141	71	71.70
	50	1.395	44.0	0.844	169	60	79.58
	75	.868	67.4	0.840	140	59	86.65
	100	.884	114.4	0.895	94	54	92.07

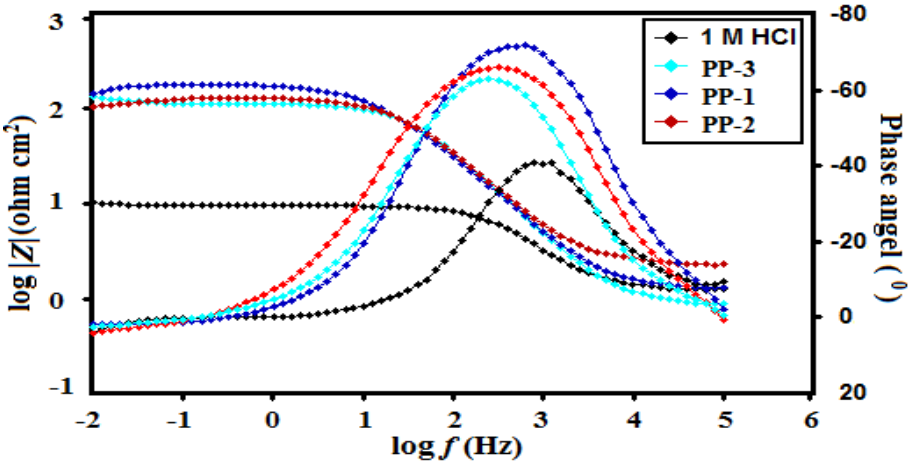

Figure 8: Bode (log f vs log $|Z|$) and phase angle (log f vs α) plots of impendence spectra for mild steel in 1M HCl in presence of different concentrations of PP derivatives

3. Mechanism of adsorption and inhibition

The corrosion prevention of MS in presence of PP derivatives can understand by adsorption mechanism. The inhibition involves blockage of the MS surface by the inhibitor molecules. Pictorial representation of the proposed mode of adsorption of PP-1 molecule is shown in Figure 9. The adsorption process was affected by the chemical structures of the inhibitors, the nature and charged surface of the metal, the distribution of charge over the whole inhibitor molecule and the type of electrolyte. Due to the complex nature of adsorption and inhibition of inhibitor, it is impossible for single adsorption mode between inhibitor and MS surface [31-33]. The inhibitor molecules may adsorb on the metal/acid solution interface by the following ways:

Figure 9: Pictorial representation of mechanism of adsorption of PP-1 on MS surface

(a) Electrostatic interaction between the protonated PPs molecules and adsorbed Cl^- on MS surface (physisorption).
(b) Interaction of unshared electron pair of PPs with the vacant d orbital of Fe atoms (chemisorption).
(c) Interaction of d-electron of iron atoms to the vacant orbital of inhibitor molecule (retrodonation)**.**

Conclusions

The results obtained for PP derivatives showed that they are good inhibitors. The potentiodynamic polarization data indicated that PP derivatives are of mixed type inhibitor.Electrochemical impedance spectroscopy data reveals the inhibition of corrosion on getting adsorbed on the MS surface. The adsorption of the inhibitor molecules on the MS surface was found to obey the Langmuir adsorption isotherm. All these data support good inhibition activity of PP derivatives.

Acknowledgements

Priyanka Singh is thankful to University Grants Commission (UGC), New Delhi for the Project (40-101/2011) SR, Fellowship.

References

1. Cui C., Zhu C., Du X. J., Wang Z. P., Li Z. M., Zhao W. G. *Green Chem*. 14 (2012) 3157
2. Dandia A., Bhati D. S., Jain A. K., Sharma G. N. *Ultrason. Sonochem*. 18 (2011) 1143
3. Chavatte P., Yous S., Marot C., Baurin N., Lesieur D. *J. Med. Chem*. 44 (2001) 3223
4. (a) Stika C. S., Gross G. A., Leguizamon G., Gerber S., Levy R., Mathur A., Bernhard L.M., Nelson D. M., Sadovsky Y., *Am. J. Obstet. Gynecol*. 187 (2002) 653.(b) Dilger K., Herrlinger C., Peters J., Seyberth H. W., Scheweer H., Klotz U. *J. Clin. Pharmacol*. 42 (2002) 985
5. Fong T. M., Heymsfield S.B. *Int. J. Obes.* 33 (2009) 947
6. Bristow D. R., Martin I. L. *J. Neurochem.* 54 (1990)751
7. Young R., Glennon R. A., Dewey W. L. *Psychopharmacology* 93(1987) 494
8. Fekry A. M., Ameer M. A. *Int. J. Hydrogen Energy* 35 (2010) 7641
9. Quartarone G., Ronchin L., Vavasori A., Tortato C., Bonaldo L. *Corros. Sci*. 64 (2012) 82
10. Vishwanatham S., Haldar N. *Corros. Sci*. 50 (2008) 2999
11. Ostovari A., Hoseinieh S. M., Peikari M., Shadizadeh S. R., Hashemi S. J. *Corros. Sci.* 51 (2009) 1935
12. Amin M. A., Abd El Rehim S. S., Abdel-Fatah H. T. M. *Corros. Sci.* 51 (2009) 882
13. Umoren S. A., Ogbobe O., Igwe I. O., Ebenso E. E. *Corros. Sci*. 50 (2008) 1998
14. Luo Y. R.Y., Zhang K., Zhu G., Tan X. *Corros. Sci*. 50 (2008) 3147
15. Li X., Deng S., Fu H. *Corros. Sci*. 53 (2011) 3241
16. De Souza F. S., Spinelli A. *Corros. Sci.*, 51 (2009) 642
17. Singh P., Quraishi M. A., Ebenso E. E. *Int. J. Electrochem. Sci*. 7 (2012) 12270
18. Rahmati A. *Tetrahedron Lett*. 51 (2010) 2967
19. Ashassi-Sorkhabi H., Seifzadeh D., Hosseini M. G. *Corros. Sci.*, 50 (2008) 3363
20. Hosseini S. M. A., Azimi A. *Corros. Sci.* 51 (2009) 728
21. Ahamad I., Prasad R., Quraishi M. A. *Corros. Sci*. 52 (2010) 933
22. Ahamad I., Quraishi M. A. *Corros. Sci.* 52 (2010) 651
23. Issaadi S., Douadi T., Zouaoui A., Chafaa S., Khan M. A., Bouet G. *Corros. Sci.* 53 (2011) 1484
24. Khaled K. F. *Appl. Surf. Sci*. (2004) 230 307
25. Ferreira E. S., Giancomelli C., Giacomelli F. C., Spinelli A. *Mater. Chem. Phys.* 83 (2004) 129
26. Amin M. A., Khaled K. F., Mohsen Q., Arida H. A. *Corros. Sci*. 52 (2010) 1684
27. Hegazy M. A., Ahmed H. M., El-Tabei A. S. *Corros. Sci.* (2011) 53 671
28. Yadav D. K., Quraishi M. A., Maiti, B. *Corros. Sci.* (2010) 52 3586
29. Deng S., Li X. *Corros. Sci*. 55(2012) 407
30. Yadav D. K., Quraishi M. A., Maiti B. *Corros. Sci.* 55 (2012) 254
31. Ahamad I., Prasad R., Quraishi M. A. *Corros. Sci.* 52 (2010) 3033
32. Ahamad I., Prasad R., Quraishi M. A. *Corros. Sci.* 52 (2010) 1472
33. Yadav D. K., Quraishi M. A. *Ind. Eng. Chem. Res*. 51 (2012) 14966